

AN INVESTIGATION ON NUMERICAL CHARACTERIZATION OF SCATTERING FROM TARGET IN A DIELECTRIC ROUGH SOIL SURFACE

Yu Liang^{1, *}, Xiang-Hua Zeng¹, Li-Xin Guo², and Zhen-Sen Wu²

¹College of Physics Science and Technology, Yangzhou University, No. 88, South University Ave., Yangzhou, Jiangsu, China

²School of Science, Xidian University, No. 2, Taibai Road, Xi'an, Shaanxi, China

Abstract—Based on the Propagation-Inside-Layer Expansion (PILE) and Forward-Backward method (FBM), the composite scattering from the target below a dielectric rough soil surface using the extended PILE (EPILE) combined with the Forward-Backward method (FBM) is studied. The accuracy and efficiency of the EPILE + FBM for this specific type of composite scattering is researched by comparing with the method of moments (MOM), the influences of the target size, target depth, target horizontal distance, the rms height, the correlation length, the incident angle and the soil moisture content, etc., to the bistatic scattering coefficient (BSC) are also investigated.

1. INTRODUCTION

The scattering from random rough surface has been one important research subject over the past several decades as its important applications in many domains, such as electromagnetics, applied optics, remote sensing, oceanography, communications, material science. As a whole, methods in studying the rough surface scattering can be categorized into two kinds: (a) the approximate, analytical methods; (b) the numerical methods. The approximate methods mainly include: the small-perturbation method (SPM) [1], the Kirchhoff or tangent plane approximation (KA) [2], the physical optics (PO) method, the two-scale method (TSM) [3], the phase perturbation method (PPM) [4], the small-slope approximation

Received 16 January 2013, Accepted 26 April 2013, Scheduled 5 May 2013

* Corresponding author: Yu Liang (liangyu@yzu.edu.cn).

(SSA) [5], etc. The numerical methods mainly include: the method of moments (MOM) [6], finite difference time domain (FDTD) [7] method, finite element method (FEM) [8], method of multiple interactions (MOMI), Banded-Matrix-Iterative-Approach/Canonical Grid (BMIA/CAG) [9], forward-backward method (FBM) [10], fast multipole method (FMM) [11,12], curvilinear coordinate (C) method [13], etc.

Since the analytical and numerical methods for studying single rough surface scattering have been very abundant, recently, the composite scattering from targets and rough surface has becoming an interest subject gradually, as its important value in many fields, such as target recognition, electronic countermeasure (ECM), ocean remote sensing, communications, etc. For the targets and rough surface composite scattering, considerable contributions have been made and several methods have been presented during these years, such as MOM [14, 15], parallel MOM [16], finite-element (FEM) method [17], finite difference time domain (FDTD) method [18], hybrid SPM/MOM technique [19], hybrid KA/MOM technique [20], hybrid PO/MOM technique [21], reciprocity theorem [22], Generalized forward-backward method (GFBM) [23, 24], Mode-expansion method [25], fast iterative approach [26], bidirectional analytic ray tracing method [27], etc. Although the aforementioned numerical methods are of respective important advantages, but some of them are fast but not exact enough, or some of them are exact but not fast enough, therefore, it should be make sense in contributing efforts to investigate and attempt to improve the efficiency and accuracy of the adoptive scheme.

In 2006, a fast numerical method, Propagation-Inside-Layer Expansion (PILE) was presented by Déchamps et al. [28]. This method is demonstrated of reasonable efficiency and exactness, and it is a method able to handle problems for the configuration with a great number of unknowns. In the beginning, the PILE was devoted to the scattering by layered rough surface [28], later, the Extended PILE (EPILE) combined with the Forward-Backward method (FBM) to study the scattering by an object above a randomly rough surface was presented by Kubické et al. [29], which can be abbreviated as the EPILE + FBM. In this paper, we attempt to use these schemes for studying the scattering by a target below a given dielectric rough soil surface, for this specific type of rough surface, more parameters, such as the moisture content of the soil, the temperature of the soil, the volumetric sand content of the soil, and the volumetric clay content of the soil, are included, which should be un-owned by the classical Gaussian spectrum rough surface, etc., then, for this specific composite configuration, efforts are made in modelling, formulating, deriving,

numerically investigating in the efficiency, accuracy, and influence of the variational parameters and their corresponding conclusions.

This paper is organized as follows. In Section 2, the geometry of the problem is defined. In Section 3, the basic formulas of the composite problem and the scattering coefficient expression are given. In Section 4, the EPILE+FBM derivation for the composite scattering problem is presented. In Section 5, the Relative Residual Error (RRE) and the computational complexity of the scheme are discussed. In Section 6, comparing with the MOM (CGM), numerical results are exhibited and other detailed discussions are given. Finally, concluding remarks are addressed.

2. GEOMETRY OF THE COMPOSITE PROBLEM

As shown in Fig. 1, a target (configuration arbitrary) is located below the rough soil surface. The problem is assumed to be two-dimensional (variant in the x - z plane). k_i represents the propagation vector of the incident wave. θ_i is the incident angle. X is the horizontal distance between the center of the target and rough soil surface (z axis). R is the size of the target. D is the vertical depth between the target and rough surface (x axis). Region $\Omega_0(\epsilon_0, \mu_0)$ denotes the free space above the rough soil surface and region $\Omega_1(\epsilon_1, \mu_1)$ denotes the space below the rough soil surface. The permittivity ϵ_1 of the soil is determined by the frequency, the rms height δ , the correlation length l , the moisture content, the temperature, the volumetric sand content, the volumetric clay content, etc. [30]. To simplify the computational condition, we assume $\mu_1 = \mu_0$, where μ_0, μ_1 denotes the relative permeability in the vacuum, in the rough soil, respectively.

The random rough soil surface is generated by the Monte-Carlo

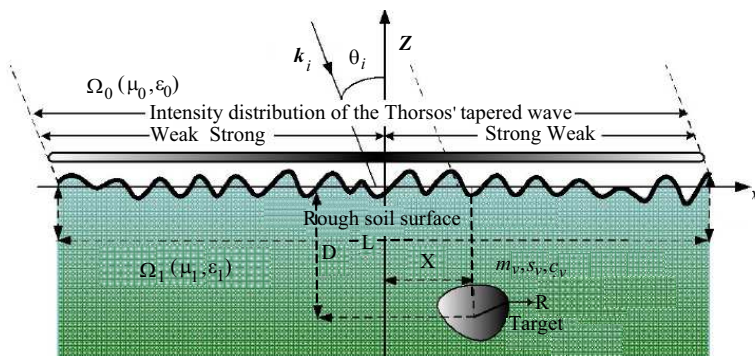


Figure 1. Geometric model of target located below the dielectric rough soil surface.

spectral method [31]. The exponential spectrum $W(K_i) = \sqrt{2\pi}\delta^2 l^2(1 + K_i^2 l^2)^{3/2}$ is applied to model the rough soil surface. K_i is the space wavenumber [31]. L is the length of the rough soil surface. The m_ν , s_ν , c_ν is the moisture content, the volumetric sand content, and the volumetric clay content of the soil, respectively. Each point of the rough soil surface, of the target will be denoted by the two dimensional position vector $\mathbf{r}_r = x_r \hat{\mathbf{x}} + z_r \hat{\mathbf{z}}$, $\mathbf{r}_t = x_t \hat{\mathbf{x}} + z_t \hat{\mathbf{z}}$, where x_r , x_t is the discretized abscissa and z_r , z_t is the discretized height. The number of samples for the target, for the rough soil surface will be denoted by N_t and N_r . To avoid edge limitations, the incident field $\varphi_{inc}(\mathbf{r})$ is chosen as the Thorsos' tapered plane wave [32] as follow

$$\varphi_{inc}(\mathbf{r}) = \exp(i\mathbf{k}_i \cdot \mathbf{r} (1 + [2(x + z \tan \theta_i)^2 - 1/g^2] / (kg \cos \theta_i)^2)) \exp(-(x + z \tan \theta_i)^2/g^2) \quad (1)$$

in which g is the tapered parameter [32]. The $e^{-i\omega t}$ time-harmonic convention is assumed and suppressed throughout this paper.

3. FORMULATION OF THE COMPOSITE PROBLEM

Considering a transverse magnetic (TM) wave $\varphi_{inc}(\mathbf{r})$ impinges on the dielectric rough soil surface, as shown in Fig. 1. According to the Ewald-Oseen' extinction theorem and the boundary conditions on the rough surface and target [14], the following integral equations can be obtained

$$\begin{aligned} \frac{1}{2}\psi_0(\mathbf{r}) - \int_{S_s} \left[\psi_0(\mathbf{r}') \frac{\partial G_0(\mathbf{r}, \mathbf{r}')}{\partial n'} - G_0(\mathbf{r}, \mathbf{r}') \frac{\partial \psi_0(\mathbf{r}')}{\partial n'} \right] ds' &= \psi_i(\mathbf{r}) \quad \mathbf{r} \in S_s \quad (2) \\ \frac{1}{2}\psi_1(\mathbf{r}) + \int_{S_s} \left[\psi_1(\mathbf{r}') \frac{\partial G_1(\mathbf{r}, \mathbf{r}')}{\partial n'} - G_1(\mathbf{r}, \mathbf{r}') \frac{\partial \psi_1(\mathbf{r}')}{\partial n'} \right] ds' \\ + \int_{S_t} \psi_1(\mathbf{r}') \frac{\partial G_1(\mathbf{r}, \mathbf{r}')}{\partial n'} ds' &= 0 \quad \mathbf{r} \in S_s \quad (3) \end{aligned}$$

$$\begin{aligned} \frac{1}{2}\psi_1(\mathbf{r}) + \int_{S_s} \left[\psi_1(\mathbf{r}') \frac{\partial G_1(\mathbf{r}, \mathbf{r}')}{\partial n'} - G_1(\mathbf{r}, \mathbf{r}') \frac{\partial \psi_1(\mathbf{r}')}{\partial n'} \right] ds' \\ + \int_{S_t} \psi_1(\mathbf{r}') \frac{\partial G_1(\mathbf{r}, \mathbf{r}')}{\partial n'} ds' &= 0 \quad \mathbf{r} \in S_t \quad (4) \end{aligned}$$

The use of the method of moments (MOM) [14] leads to the following linear system

$$\bar{\mathbf{Z}}_{(2N_s+N_t) \times (2N_s+N_t)} \mathbf{X}_{(2N_s+N_t)} = \mathbf{S}_{(2N_s+N_t)} \quad (5)$$

in which $\bar{\mathbf{Z}}_{(2N_s+N_t) \times (2N_s+N_t)}$ denotes the impedance matrix, $\mathbf{X}_{(2N_s+N_t)}$ is the induced unknown vector, $\mathbf{S}_{(2N_s+N_t)}$ is the incident source item.

The impedance matrix is expressed as

$$\bar{\mathbf{Z}} = \begin{bmatrix} \mathbf{A}_{N_s \times N_s} & \mathbf{B}_{N_s \times N_s} & \mathbf{0}_{N_s \times N_t} \\ \mathbf{C}_{N_s \times N_s} & -\rho \mathbf{D}_{N_s \times N_s} & \mathbf{E}_{N_s \times N_t} \\ \mathbf{F}_{N_t \times N_s} & -\rho \mathbf{G}_{N_t \times N_s} & \mathbf{H}_{N_t \times N_t} \end{bmatrix} \quad (6)$$

with $\rho = \varepsilon_1/\varepsilon_0$. $\bar{\mathbf{Z}}$ can be divided into four blocks and expressed as follow

$$\bar{\mathbf{Z}} = \begin{bmatrix} \bar{\mathbf{A}}_{(2N_s) \times (2N_s)}^s & \bar{\mathbf{A}}_{(2N_s) \times (N_t)}^{t \rightarrow s} \\ \bar{\mathbf{A}}_{(N_t) \times (2N_s)}^{s \rightarrow t} & \bar{\mathbf{A}}_{(N_t) \times (N_t)}^t \end{bmatrix} \quad (7)$$

where

$$\bar{\mathbf{A}}_{(2N_s) \times (2N_s)}^s = \begin{bmatrix} \mathbf{A}_{N_s \times N_s} & \mathbf{B}_{N_s \times N_s} \\ \mathbf{C}_{N_s \times N_s} & -\rho \mathbf{D}_{N_s \times N_s} \end{bmatrix}, \quad \bar{\mathbf{A}}_{(2N_s) \times (N_t)}^{t \rightarrow s} = \begin{bmatrix} \mathbf{0}_{N_s \times N_t} \\ \mathbf{E}_{N_s \times N_t} \end{bmatrix} \quad (8)$$

$$\bar{\mathbf{A}}_{(N_t) \times (2N_s)}^{s \rightarrow t} = [\mathbf{F}_{N_t \times N_s} \quad -\rho \mathbf{G}_{N_t \times N_s}], \quad \bar{\mathbf{A}}_{(N_t) \times (N_t)}^t = [\mathbf{H}_{N_t \times N_t}] \quad (9)$$

$\bar{\mathbf{A}}_{(2N_s) \times (2N_s)}^s$ corresponds exactly to the impedance matrix of the rough soil surface, $\bar{\mathbf{A}}_{(2N_s) \times (N_t)}^{t \rightarrow s}$ and $\bar{\mathbf{A}}_{(N_t) \times (2N_s)}^{s \rightarrow t}$ can be interpreted as coupling matrices between the target and the rough soil surface, $\bar{\mathbf{A}}_{(N_t) \times (N_t)}^t$ corresponds exactly to the impedance matrix of the target. The unknown vector and the source item are defined as follows

$$\mathbf{X}_{(2N_s+N_t)}^T = \begin{bmatrix} \mathbf{X}_{s(2N_s)}^T & \mathbf{X}_{t(N_t)}^T \end{bmatrix}, \quad \mathbf{S}_{(2N_s+N_t)}^T = \begin{bmatrix} \mathbf{S}_{s(2N_s)}^T & \mathbf{S}_{t(N_t)}^T \end{bmatrix} \quad (10)$$

with

$$\mathbf{X}_{s(2N_s)}^T = \begin{bmatrix} \underbrace{\psi_0(\mathbf{r}_s^1) \cdots \psi_0(\mathbf{r}_s^N)}_{N_s} \quad \underbrace{\frac{\partial \psi_0(\mathbf{r}_s^1)}{\partial n_s} \cdots \frac{\partial \psi_0(\mathbf{r}_s^N)}{\partial n_s}}_{N_s} \end{bmatrix}, \quad (11)$$

$$\mathbf{X}_{t(N_t)}^T = \begin{bmatrix} \underbrace{\psi_1(\mathbf{r}_t^1) \cdots \psi_1(\mathbf{r}_t^N)}_{N_t} \end{bmatrix}$$

$$\mathbf{S}_{s(2N_s)}^T = \begin{bmatrix} \underbrace{\psi_i(\mathbf{r}_s^1) \cdots \psi_i(\mathbf{r}_s^N)}_{N_s} \quad \underbrace{0 \cdots 0}_{N_s} \end{bmatrix}, \quad \mathbf{S}_{t(N_t)}^T = \begin{bmatrix} \underbrace{0 \cdots 0}_{N_t} \end{bmatrix} \quad (12)$$

in which the superscript T stands for the transpose operator, and $\partial/\partial n$ stands for the normal derivative operator. The elements of the

impedance matrix $\bar{\mathbf{Z}}_{(2N_s+N_t) \times (2N_s+N_t)}$ are shown below

$$A_{mn} = \begin{cases} \frac{-jk_0\gamma_n\Delta x_s}{4}(\hat{\mathbf{n}}_s \cdot \mathbf{R}_{mn})H_1^{(1)}(k_0|\mathbf{r}_m - \mathbf{r}_n|) & m \neq n \\ \frac{1}{2} - \frac{f''(x_m)\Delta x_s}{4\pi\gamma_m^2} & m = n \end{cases}, \quad (13)$$

$$B_{mn} = \begin{cases} \frac{j\gamma_n\Delta x_s}{4}H_0^{(1)}(k_0|\mathbf{r}_m - \mathbf{r}_n|) & m \neq n \\ \frac{j\gamma_m\Delta x_s}{4}H_0^{(1)}\left[\frac{k_0\Delta x_s\gamma_m}{2e}\right] & m = n \end{cases}$$

$$C_{mn} = \begin{cases} \frac{jk_1\gamma_n\Delta x_s}{4}(\hat{\mathbf{n}}_s \cdot \mathbf{R}_{mn})H_1^{(1)}(k_1|\mathbf{r}_m - \mathbf{r}_n|) & m \neq n \\ \frac{1}{2} + \frac{f''(x_m)\Delta x_s}{4\pi\gamma_m^2} & m = n \end{cases}, \quad (14)$$

$$D_{mn} = \begin{cases} \frac{j\gamma_n\Delta x_s}{4}H_0^{(1)}(k_1|\mathbf{r}_m - \mathbf{r}_n|) & m \neq n \\ \frac{j\gamma_m\Delta x_s}{4}H_0^{(1)}\left[\frac{k_1\Delta x_s\gamma_m}{2e}\right] & m = n \end{cases}$$

$$E_{mp} = \gamma_p\Delta x_t \frac{jk_1}{4}(\hat{\mathbf{n}}_t \cdot \mathbf{R}_{mp})H_1^{(1)}(k_1|\mathbf{r}_m - \mathbf{r}_p|), \quad (15)$$

$$F_{qn} = \gamma_n\Delta x_s \frac{jk_1}{4}(\hat{\mathbf{n}}_s \cdot \mathbf{R}_{qn})H_1^{(1)}(k_1|\mathbf{r}_q - \mathbf{r}_n|)$$

$$G_{qn} = -\gamma_n\Delta x_s \frac{j}{4}H_0^{(1)}(k_1|\mathbf{r}_q - \mathbf{r}_n|),$$

$$H_{qp} = \begin{cases} \gamma_p\Delta x_t \frac{jk_1}{4}(\hat{\mathbf{n}}_t \cdot \mathbf{R}_{qp})H_1^{(1)}(k_1|\mathbf{r}_q - \mathbf{r}_p|) & q \neq p \\ \frac{1}{2} + \frac{Z_t''(x_p)\Delta x_t}{4\pi\gamma_p^2} & q = p \end{cases} \quad (16)$$

$k_0 = 2\pi/\lambda$ is the wavenumber in the free space, λ the incident wave length, and $k_1 = k_0\sqrt{\varepsilon_1}$ the wavenumber in the incident medium Ω_1 . Δx_t and Δx_s are the sampling steps for the target and rough soil surface, the arbitrary two points of the target or the rough soil surface are denoted by $\mathbf{r}_{p/q} = x_{p/q}\hat{\mathbf{x}} + z_{p/q}\hat{\mathbf{z}}$ and $\mathbf{r}_{m/n} = x_{m/n}\hat{\mathbf{x}} + z_{m/n}\hat{\mathbf{z}}$, the $z_t''(x_{p/q})$ and $f''(x_{m/n})$ are second-order differential of height function of the target, the rough surface, respectively. $e = 2.718214$, $\gamma = 1.781072$, $H_0^{(1)}$, $H_1^{(1)}$ denotes the zeroth, the first-order Hankel function. In Eqs. (13)–(16) the variables γ_n , γ_m , $\hat{\mathbf{n}}_t$, γ_p , γ_q and \mathbf{R}_{ij} are defined as follows

$$\gamma_n = \sqrt{1 + [f'(x_n)]^2}, \quad \gamma_m = \sqrt{1 + [f'(x_m)]^2}, \quad \hat{\mathbf{n}}_t = \frac{-z_t'(x_p)\hat{\mathbf{x}} + \hat{\mathbf{z}}}{\sqrt{1 + [z_t'(x_p)]^2}} \quad (17)$$

$$\begin{aligned} \gamma_p &= \sqrt{1 + [z'_t(x_p)]^2}, \quad \gamma_q = \sqrt{1 + [z'_t(x_q)]^2}, \\ \mathbf{R}_{ij} &= \frac{\mathbf{r}_i - \mathbf{r}_j}{|\mathbf{r}_i - \mathbf{r}_j|} \quad i = m, q; \quad j = n, p \end{aligned} \tag{18}$$

From the Huygens formula [31], the scattering field in the free space is given by

$$\psi_s(\mathbf{r}) = \frac{e^{jk_0r}}{\sqrt{r}} \psi_s^N(\theta_s, \theta_i) \tag{19}$$

where

$$\begin{aligned} \psi_s^N(\theta_s, \theta_i) &= \frac{j}{4} \sqrt{\frac{2}{\pi k_0}} e^{-j\frac{\pi}{4}} \left\{ \int_{S_s} [-j(\hat{\mathbf{n}}_s \cdot \mathbf{k}_s) V_1(x) - V_2(x)] \right. \\ &\quad \left. \cdot \exp(-j\mathbf{k}_s \cdot \mathbf{r}) \sqrt{1 + [f'(x)]^2} dx \right\} \end{aligned} \tag{20}$$

in which, V_1 equals $\mathbf{X}_{s(1 \sim N_s)}^T$, and V_2 corresponds to $\mathbf{X}_{s(N_s \sim 2N_s)}^T$. The expression for the normalized far-field composite bistatic scattering coefficient (BSC) with the Thorsos' tapered plane wave incidence is given as follow

$$\sigma_s(\theta_s, \theta_i) = \frac{|\psi_s^N(\theta_s, \theta_i)|^2}{g\sqrt{\frac{\pi}{2}} \cos \theta_i \left(1 - \frac{1+2 \tan^2 \theta_i}{2k_0^2 g^2 \cos^2 \theta_i}\right)} \tag{21}$$

Usually, when the number of sampling for the target, for the rough soil surface increases, the computational cost of solving the matrix equation using the conjugate gradient method (CGM) [33] or biconjugate gradient method (BCGM) or the direct LU inversion becomes prohibitive, in the following section, the efficient numerical method, i.e., the EPILE + FBM is adopted to speed up the scattering calculation.

4. DERIVATION BY THE EXTENDED PROPAGATION INSIDE LAYER EXPANSION COMBINED WITH FORWARD-BACKWARD METHOD

Déchamps et al. have presented the PILE to investigate the layer rough surface scattering [28], then, the Extended PILE (EPILE) to research the scattering from a target above the rough surface was presented by Kubické et al. [29], and we also have attempted to combine the EPILE with generalized FBM for targets above and on the rough surface problem [24], herein, according to these

schemes [24, 28, 29], the inverse matrix of $\bar{\mathbf{Z}}$ is partitioned into four blocks as follow

$$\bar{\mathbf{Z}}_{(2N_s+N_t)\times(2N_s+N_t)}^{-1} = \begin{bmatrix} \bar{\mathbf{T}} & \bar{\mathbf{U}} \\ \bar{\mathbf{V}} & \bar{\mathbf{W}} \end{bmatrix} \quad (22)$$

where

$$\bar{\mathbf{T}} = [\bar{\mathbf{A}}_{(2N_s)\times(2N_s)}^s - \bar{\mathbf{A}}_{(2N_s)\times N_t}^{t\rightarrow s} \cdot (\bar{\mathbf{A}}_{N_t\times N_t}^t)^{-1} \cdot \bar{\mathbf{A}}_{N_t\times(2N_s)}^{s\rightarrow t}]^{-1} \quad (23)$$

$$\begin{aligned} \bar{\mathbf{U}} = & -[\bar{\mathbf{A}}_{(2N_s)\times(2N_s)}^s - \bar{\mathbf{A}}_{(2N_s)\times N_t}^{t\rightarrow s} \cdot (\bar{\mathbf{A}}_{N_t\times N_t}^t)^{-1} \cdot \bar{\mathbf{A}}_{N_t\times(2N_s)}^{s\rightarrow t}]^{-1} \\ & \cdot \bar{\mathbf{A}}_{(2N_s)\times N_t}^{t\rightarrow s} \cdot (\bar{\mathbf{A}}_{N_t\times N_t}^t)^{-1} \end{aligned} \quad (24)$$

$$\begin{aligned} \bar{\mathbf{V}} = & -(\bar{\mathbf{A}}_{N_t\times N_t}^t)^{-1} \cdot \bar{\mathbf{A}}_{N_t\times(2N_s)}^{s\rightarrow t} \cdot [\bar{\mathbf{A}}_{(2N_s)\times(2N_s)}^s - \bar{\mathbf{A}}_{(2N_s)\times N_t}^{t\rightarrow s} \\ & \cdot (\bar{\mathbf{A}}_{N_t\times N_t}^t)^{-1} \cdot \bar{\mathbf{A}}_{N_t\times(2N_s)}^{s\rightarrow t}]^{-1} \end{aligned} \quad (25)$$

$$\begin{aligned} \bar{\mathbf{W}} = & (\bar{\mathbf{A}}_{N_t\times N_t}^t)^{-1} - (\bar{\mathbf{A}}_{N_t\times N_t}^t)^{-1} \cdot \bar{\mathbf{A}}_{N_t\times(2N_s)}^{s\rightarrow t} \cdot [\bar{\mathbf{A}}_{(2N_s)\times(2N_s)}^s - \bar{\mathbf{A}}_{(2N_s)\times N_t}^{t\rightarrow s} \\ & \cdot (\bar{\mathbf{A}}_{N_t\times N_t}^t)^{-1} \cdot \bar{\mathbf{A}}_{N_t\times(2N_s)}^{s\rightarrow t}]^{-1} \cdot \bar{\mathbf{A}}_{(2N_s)\times N_t}^{t\rightarrow s} \cdot (\bar{\mathbf{A}}_{N_t\times N_t}^t)^{-1} \end{aligned} \quad (26)$$

The total induced unknown vector on the rough soil surface can be expressed as follow

$$\begin{aligned} \mathbf{X}_s = & [\bar{\mathbf{A}}_{(2N_s)\times(2N_s)}^s - \bar{\mathbf{A}}_{(2N_s)\times N_t}^{t\rightarrow s} \cdot (\bar{\mathbf{A}}_{N_t\times N_t}^t)^{-1} \\ & \cdot \bar{\mathbf{A}}_{N_t\times(2N_s)}^{s\rightarrow t}]^{-1} \cdot \mathbf{S}_s \end{aligned} \quad (27)$$

The total induced unknown vector on the target can be expressed as follow

$$\begin{aligned} \mathbf{X}_t = & -(\bar{\mathbf{A}}_{N_t\times N_t}^t)^{-1} \bar{\mathbf{A}}_{N_t\times(2N_s)}^{s\rightarrow t} [\bar{\mathbf{A}}_{(2N_s)\times(2N_s)}^s \\ & - \bar{\mathbf{A}}_{(2N_s)\times N_t}^{t\rightarrow s} \cdot (\bar{\mathbf{A}}_{N_t\times N_t}^t)^{-1} \cdot \bar{\mathbf{A}}_{N_t\times(2N_s)}^{s\rightarrow t}]^{-1} \cdot \mathbf{S}_s \end{aligned} \quad (28)$$

Introducing the characteristic matrix $\mathbf{M}_{c(s)}$ on the rough soil surface as follow

$$\mathbf{M}_{c(s)} = (\bar{\mathbf{A}}_{(2N_s)\times(2N_s)}^s)^{-1} \cdot \bar{\mathbf{A}}_{(2N_s)\times N_t}^{t\rightarrow s} \cdot (\bar{\mathbf{A}}_{N_t\times N_t}^t)^{-1} \cdot \bar{\mathbf{A}}_{N_t\times(2N_s)}^{s\rightarrow t} \quad (29)$$

Similarly, introducing the characteristic matrix $\mathbf{M}_{c(t)}$ on the target as follow

$$\mathbf{M}_{c(t)} = (\bar{\mathbf{A}}_{N_t\times N_t}^t)^{-1} \cdot \bar{\mathbf{A}}_{N_t\times(2N_s)}^{s\rightarrow t} \cdot (\bar{\mathbf{A}}_{(2N_s)\times(2N_s)}^s)^{-1} \cdot \bar{\mathbf{A}}_{(2N_s)\times N_t}^{t\rightarrow s} \quad (30)$$

Defining the norm $\|\cdot\|$ of \mathbf{M}_c by its spectral radius [28], and if $\|\mathbf{M}_c\| < 1$, then, from Eqs. (27) and (29), the total induced vector on the rough surface can be expressed as

$$\mathbf{X}_{s(2N_s)}^{(p)} = \left(\sum_{p=0}^P \mathbf{M}_c^p \right) \cdot (\bar{\mathbf{A}}_{(2N_s)\times(2N_s)}^s)^{-1} \cdot \mathbf{S}_s = \sum_{p=0}^P \mathbf{Y}_s^{(p)} \quad (31)$$

where $\sum_{p=0}^P \mathbf{M}_c^p = \bar{\mathbf{I}} - (\bar{\mathbf{A}}_{N_t \times N_t}^t)^{-1} \bar{\mathbf{A}}_{(2N_s) \times N_t}^{t \rightarrow s} (\bar{\mathbf{A}}_{(2N_s) \times (2N_s)}^s)^{-1} \bar{\mathbf{A}}_{N_t \times (2N_s)}^{s \rightarrow t}$,

$\bar{\mathbf{I}}$ is the identity matrix.

From Eqs. (28) and (30), the total induced vector on the target can be expressed as

$$\begin{aligned} \mathbf{X}_{t(N_t)}^{(p)} &= -(\bar{\mathbf{A}}_{N_t \times N_t}^t)^{-1} \bar{\mathbf{A}}_{N_t \times (2N_s)}^{s \rightarrow t} \left(\sum_{p=0}^P \mathbf{M}_c^p \right) \cdot (\bar{\mathbf{A}}_{(2N_s) \times (2N_s)}^s)^{-1} \cdot \mathbf{S}_s \\ &= -(\bar{\mathbf{A}}_{N_t \times N_t}^t)^{-1} \bar{\mathbf{A}}_{N_t \times (2N_s)}^{s \rightarrow t} \sum_{p=0}^P \mathbf{Y}_s^{(p)} \end{aligned} \quad (32)$$

Therefore, $\mathbf{X}_{s(2N_s)}^{(p)}$ and $\mathbf{X}_{t(N_t)}^{(p)}$ can be expressed as follows

$$\mathbf{X}_{s(2N_s)}^{(p)} = \sum_{p=0}^P \mathbf{Y}_s^{(p)}, \quad \mathbf{X}_{t(N_t)}^{(p)} = -(\bar{\mathbf{A}}_{N_t \times N_t}^t)^{-1} \bar{\mathbf{A}}_{N_t \times (2N_s)}^{s \rightarrow t} \sum_{p=0}^P \mathbf{Y}_s^{(p)} \quad (33)$$

Each item in expressions above is given below

$$\mathbf{Y}_s^{(0)} = (\bar{\mathbf{A}}_{(2N_s) \times (2N_s)}^s)^{-1} \cdot \mathbf{S}_s, \quad \mathbf{Y}_s^{(p)} = \mathbf{M}_{c(s)} \cdot \mathbf{Y}_s^{(p-1)} \quad (34)$$

p denotes the iteration order. In Eqs. (29) and (30), the $(\bar{\mathbf{A}}_{N_t \times N_t}^t)^{-1}$ accounts for the local interactions on the target, $(\bar{\mathbf{A}}_{(2N_s) \times (2N_s)}^s)^{-1}$ accounts for the local interactions on the rough soil surface, $\bar{\mathbf{A}}_{N_t \times (2N_s)}^{s \rightarrow t}$ propagates the resulting field on the rough soil surface toward the target (downward coupling), $\bar{\mathbf{A}}_{(2N_s) \times N_t}^{t \rightarrow s}$ propagates the resulting field on the target toward the rough soil surface (upward coupling), and so on for the subsequent terms $\mathbf{Y}_s^{(p)}$. Usually, at each iteration step, the number N_t of samples for the target is less than the number N_s of samples for the rough surface, the term $(\bar{\mathbf{A}}_{N_t \times N_t}^t)^{-1} \zeta$ (ζ denotes the unknown column vector of length N_t) will be solved by the MOM (CGM/BCGM/LU), while, to decrease the computing cost and speed up the calculation of the term $(\bar{\mathbf{A}}_{(2N_s) \times (2N_s)}^s)^{-1} \zeta_{s(2N_s)}$ (i.e., single underlying rough surface, $\zeta_{s(2N_s)}$ denotes the unknown column vector of length $2N_s$), the FBM by Iodice [10] can be applied. Assume $(\bar{\mathbf{A}}_{(2N_s) \times (2N_s)}^s)^{-1} \zeta_{s(2N_s)}$ equals $\xi_{(2N_s)}$ (ξ denotes the unknown column vector of length $2N_s$). The impedance matrix and induced unknown vector can be decomposed as follows

$$\bar{\mathbf{A}}_{s((2N_s) \times (2N_s))} = \bar{\mathbf{A}}_{s((2N_s) \times (2N_s))}^f + \bar{\mathbf{A}}_{s((2N_s) \times (2N_s))}^d + \bar{\mathbf{A}}_{s((2N_s) \times (2N_s))}^b \quad (35)$$

$$\xi_{s(2N_s)} = \xi_{s(2N_s)}^f + \xi_{s(2N_s)}^b \quad (36)$$

in which $\bar{\mathbf{A}}_s^f$, $\bar{\mathbf{A}}_s^d$ and $\bar{\mathbf{A}}_s^b$ denote the lower triangle part, the diagonal part, and the upper triangle part of $\bar{\mathbf{A}}_s$, respectively. $\xi_{s(2N_s)}^f$ and $\xi_{s(2N_s)}^b$ are the forward, backward induced unknown vector on the rough soil surface.

Assume that $\xi_{s(2N_s)} = [\xi_{1s(N_s)}^T \xi_{2s(N_s)}^T]^T$ and $\zeta_{s(2N_s)} = [\zeta_{1s(N_s)}^T \zeta_{2s(N_s)}^T]^T$, therefore,

$$\begin{bmatrix} \mathbf{A}_{N_s \times N_s} & \mathbf{B}_{N_s \times N_s} \\ \mathbf{C}_{N_s \times N_s} & -\rho \mathbf{D}_{N_s \times N_s} \end{bmatrix} \cdot \begin{bmatrix} \xi_{1s(N_s)}^T \\ \xi_{2s(N_s)}^T \end{bmatrix} = \begin{bmatrix} \zeta_{1s(N_s)}^T \\ \zeta_{2s(N_s)}^T \end{bmatrix} \quad (37)$$

That is

$$\mathbf{A}_{N_s \times N_s} = \mathbf{A}_{N_s \times N_s}^f + \mathbf{A}_{N_s \times N_s}^s + \mathbf{A}_{N_s \times N_s}^b, \quad (38)$$

$$\mathbf{B}_{N_s \times N_s} = \mathbf{B}_{N_s \times N_s}^f + \mathbf{B}_{N_s \times N_s}^s + \mathbf{B}_{N_s \times N_s}^b$$

$$\mathbf{C}_{N_s \times N_s} = \mathbf{C}_{N_s \times N_s}^f + \mathbf{C}_{N_s \times N_s}^s + \mathbf{C}_{N_s \times N_s}^b, \quad (39)$$

$$\mathbf{D}_{N_s \times N_s} = \mathbf{D}_{N_s \times N_s}^f + \mathbf{D}_{N_s \times N_s}^s + \mathbf{D}_{N_s \times N_s}^b$$

$$\begin{aligned} & \mathbf{A}_{N_s \times N_s}^s \cdot \xi_{1s(N_s)}^{T(f)} + \mathbf{B}_{N_s \times N_s}^s \cdot \xi_{2s(N_s)}^{T(f)} \\ = & \zeta_{2s(2N_s)}^T - \mathbf{A}_{N_s \times N_s}^f \cdot \left(\xi_{1s(N_s)}^{T(f)} + \xi_{1s(N_s)}^{T(b)} \right) - \mathbf{B}_{N_s \times N_s}^f \cdot \left(\xi_{2s(N_s)}^{T(f)} + \xi_{2s(N_s)}^{T(b)} \right) \end{aligned} \quad (40)$$

$$\begin{aligned} & \mathbf{C}_{N_s \times N_s}^s \cdot \xi_{1s(N_s)}^{T(f)} - \rho \mathbf{D}_{N_s \times N_s}^s \cdot \xi_{2s(N_s)}^{T(f)} \\ = & -\mathbf{C}_{N_s \times N_s}^f \cdot \left(\xi_{1s(N_s)}^{T(f)} + \xi_{1s(N_s)}^{T(b)} \right) + \rho \mathbf{D}_{N_s \times N_s}^f \cdot \left(\xi_{2s(N_s)}^{T(f)} + \xi_{2s(N_s)}^{T(b)} \right) \end{aligned} \quad (41)$$

$$\begin{aligned} & \mathbf{A}_{N_s \times N_s}^s \cdot \xi_{1s(N_s)}^{T(b)} + \mathbf{B}_{N_s \times N_s}^s \cdot \xi_{2s(N_s)}^{T(b)} \\ = & -\mathbf{A}_{N_s \times N_s}^b \cdot \left(\xi_{1s(N_s)}^{T(f)} + \xi_{1s(N_s)}^{T(b)} \right) - \mathbf{B}_{N_s \times N_s}^b \cdot \left(\xi_{2s(N_s)}^{T(f)} + \xi_{2s(N_s)}^{T(b)} \right) \end{aligned} \quad (42)$$

$$\begin{aligned} & \mathbf{C}_{N_s \times N_s}^s \cdot \xi_{1s(N_s)}^{T(b)} - \rho \mathbf{D}_{N_s \times N_s}^s \cdot \xi_{2s(N_s)}^{T(b)} \\ = & -\mathbf{C}_{N_s \times N_s}^b \cdot \left(\xi_{1s(N_s)}^{T(f)} + \xi_{1s(N_s)}^{T(b)} \right) + \rho \mathbf{D}_{N_s \times N_s}^b \cdot \left(\xi_{2s(N_s)}^{T(f)} + \xi_{2s(N_s)}^{T(b)} \right) \end{aligned} \quad (43)$$

The iterations can be carried out as follows

$$\begin{aligned} & \left(\mathbf{A}_{N_s \times N_s}^s + \mathbf{A}_{N_s \times N_s}^f \right) \cdot \xi_{1s(N_s)}^{T(f)(i)} + \left(\mathbf{B}_{N_s \times N_s}^s + \mathbf{B}_{N_s \times N_s}^f \right) \cdot \xi_{2s(N_s)}^{T(f)(i)} \\ = & \zeta_{1s(N_s)}^T - \mathbf{A}_{N_s \times N_s}^f \cdot \xi_{1s(N_s)}^{T(b)(i-1)} - \mathbf{B}_{N_s \times N_s}^f \cdot \xi_{2s(N_s)}^{T(f)(i-1)} \\ & \left(\mathbf{C}_{N_s \times N_s}^s + \mathbf{C}_{N_s \times N_s}^f \right) \cdot \xi_{1s(N_s)}^{T(f)(i)} - \rho \left(\mathbf{D}_{N_s \times N_s}^s + \mathbf{D}_{N_s \times N_s}^f \right) \cdot \xi_{2s(N_s)}^{T(f)(i)} \end{aligned} \quad (44)$$

$$= -\mathbf{C}_{N_s \times N_s}^f \cdot \xi_{1s(2N_s)}^{T(b)(i-1)} + \rho \mathbf{D}_{N_s \times N_s}^f \cdot \xi_{2s(N_s)}^{T(b)(i-1)} \quad (45)$$

$$\begin{aligned} & \left(\mathbf{A}_{N_s \times N_s}^s + \mathbf{A}_{N_s \times N_s}^b \right) \cdot \xi_{1s(N_s)}^{T(b)(i)} + \left(\mathbf{B}_{N_s \times N_s}^s + \mathbf{B}_{N_s \times N_s}^b \right) \cdot \xi_{2s(N_s)}^{T(b)(i)} \\ & = -\mathbf{A}_{N_s \times N_s}^b \cdot \xi_{1s(N_s)}^{T(f)(i)} - \mathbf{B}_{N_s \times N_s}^b \cdot \xi_{2s(N_s)}^{T(f)(i)} \end{aligned} \quad (46)$$

$$\begin{aligned} & \left(\mathbf{C}_{N_s \times N_s}^s + \mathbf{C}_{N_s \times N_s}^b \right) \cdot \xi_{1s(N_s)}^{T(b)(i)} - \rho \left(\mathbf{D}_{N_s \times N_s}^s + \mathbf{D}_{N_s \times N_s}^b \right) \cdot \xi_{2s(N_s)}^{T(b)(i)} \\ & = -\mathbf{C}_{N_s \times N_s}^b \cdot \xi_{1s(N_s)}^{T(f)(i)} + \rho \mathbf{D}_{N_s \times N_s}^b \cdot \xi_{2s(N_s)}^{T(f)(i)} \end{aligned} \quad (47)$$

i is the iteration order. Therefore, for investigating the scattering from the single rough soil surface, the FBM can be adopted; for further investigating the composite scattering from target below the rough soil surface, the EPLIE combined with FBM (i.e., EPILE + FBM) can be applied.

5. RELATIVE RESIDUAL ERROR AND COMPUTATIONAL COMPLEXITY

To validate the accuracy and efficiency of the EPILE + FBM, the Relative Residual Error (RRE) and computational complexity $o()$ are necessarily investigated [34]. The RRE of the scattering coefficient σ obtained by using the EPILE + FBM is defined as the norm of the following form

$$RRE = \frac{\sum_{i=-90}^{i=90} |\sigma_{(\text{PILE+FBM})} - \sigma_{(\text{MOM(CGM/LU/BCGM)})}|^2}{\sum_{i=-90}^{i=90} |\sigma_{\text{MOM(CGM/LU/BCGM)}}|^2} \quad (48)$$

where $\sigma_{(\text{MOM(CGM/LU/BCGM)})}$ denotes the BSC calculated by the MOM (CGM), or MOM (LU), or MOM (BCGM). The computational complexities per iteration of terms $\mathbf{Y}_t^{(p)}$, $\mathbf{Y}_s^{(p)}$ are given below

$$\begin{aligned} & \mathbf{M}_{c(s)} \cdot \mathbf{Y}_s^{(p-1)} \\ & = \underbrace{\left(\bar{\mathbf{A}}_{(2N_s) \times (2N_s)}^s \right)^{-1} \cdot \bar{\mathbf{A}}_{(2N_s) \times N_t}^{t \rightarrow s} \cdot \left(\bar{\mathbf{A}}_{N_t \times N_t}^t \right)^{-1} \cdot \underbrace{\bar{\mathbf{A}}_{N_t \times (2N_s)}^{s \rightarrow t} \cdot \mathbf{Y}_s^{(p-1)}}_{\substack{o(N_t \times (2N_s)) \quad (a) \\ o(M_{iter} 12(N_t)^2) \text{ or } o(4(N_t/3)^3) \quad (b) \\ o((2N_s) \times N_t) \quad (c) \\ o((2N_s)^2) \quad (d)}}} \end{aligned} \quad (49)$$

$$\mathbf{M}_{c(t)} \cdot \mathbf{Y}_{(t)}^{(p-1)}$$

$$\begin{aligned}
&= \underbrace{\left(\bar{\mathbf{A}}_{N_t \times N_t}^t\right)^{-1} \cdot \bar{\mathbf{A}}_{N_t \times (2N_s)}^{s \rightarrow t} \cdot \left(\bar{\mathbf{A}}_{(2N_s) \times (2N_s)}^s\right)^{-1}}_{o(N_t \times (2N_s)) \text{ (g)}} \cdot \underbrace{\bar{\mathbf{A}}_{(2N_s) \times N_t}^{t \rightarrow s}}_{o((2N_s) \times N_t) \text{ (e)}} \cdot \mathbf{Y}_{(t)}^{(p-1)} \text{ (50)} \\
&\quad \underbrace{\hspace{10em}}_{o((2N_s)^2) \text{ (f)}} \\
&\quad \underbrace{\hspace{15em}}_{o(M_{iter}12(N_t)^2) \text{ or } o(4(N_t/3)^3) \text{ (h)}}
\end{aligned}$$

Operations (a), (c), (e), (g) are matrix-vector multiplications: their computational complexities are $o(N_t \times (2N_s))$. Operations (d), (f) are the fast FBM iterative inversions: their complexities are $o((2N_s)^2)$. Operations (b) and operations (h) are the MoM (CGM) or MOM (LU) (scheme), whose complexities are $o(M_{iter}12(N_t)^2)$ or $o((4N_t/3)^3)$, where M_{iter} is the number of iterations in CGM iteration scheme. Therefore, the total complexity is $o(N_t \times (2N_s) + M_{iter}12(N_t)^2 + (2N_s) \times N_t + (2N_s)^2)$ or $o(N_t \times (2N_s) + (4N_t/3)^3 + (2N_s) \times N_t + (2N_s)^2)$ for both calculation of terms $\mathbf{Y}_t^{(p)}$ and $\mathbf{Y}_s^{(p)}$, where p is the number of iterations in the EPILE scheme, for $N_s \gg N_t$, i.e., the number of samples for the rough surface is much more than the target, or the size of the rough surface is far bigger than that of the target, the complexity is about $o(p(2N_s + (N_s)^2))$, p is generally less than 10 and M_{iter} is generally far bigger than 100, so this method is much faster than the direct LU inversion, of order $o((4N_s/3)^3)$, and the conjugate gradient scheme, of order $o(M_{iter}12(N_s)^2)$.

6. NUMERICAL RESULTS AND DISCUSSIONS

In this section, on the one hand, comparing with the MOM (CGM), the RRE and the average computational time (CT) of the ordered EPILE + FBM are discussed, the target is a two-dimensional cylinder with infinite length in y -direction; on the other hand, using the ordered PILE+FBM, with changing of target radius, target depth, rms height, correlation length, incident angle, soil moisture content, and target horizontal distance, the bistatic scattering coefficient (BSC) of the cylinder target located below rough soil surface are investigated. The aforementioned numerical algorithms are tested on the computer with a 2.33 GHz processor (Intel Core 2 Quad Q8200), 4GB Memory, ASUSTeK P5 Mainboard, Microsoft Windows XP operation system, and the Fortran PowerStation compiler. It should be noted that all the curves below are plotted in decibel (dB) scale.

The norm $\|\mathbf{M}_c\|$ versus the distance between the surface and the target is plotted in Figs. 2 and 3. Fig. 2 refers to the case that the length of rough surface is $L = 25\lambda$, and Fig. 3 is for $L = 100\lambda$.

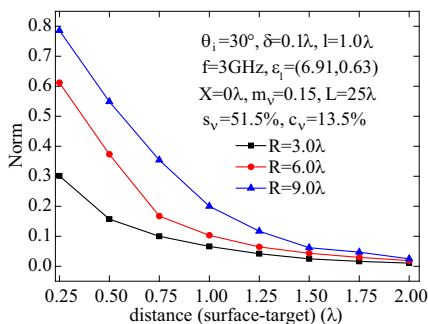


Figure 2. Norm versus distance under $L = 25\lambda$.

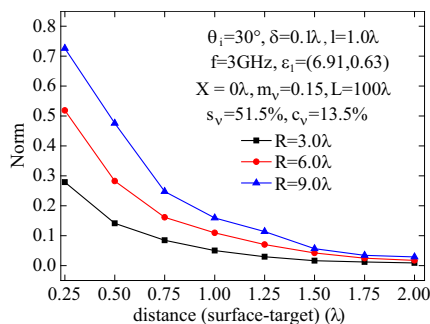


Figure 3. Norm versus distance under $L = 100\lambda$.

The incident frequency f is 3 GHz. The radius of the cylinder is denoted by R . The number of samples for the rough surface is 256 for $L = 25\lambda$, 1024 for $L = 100\lambda$. In both figures, it can be found that the norm $\|\mathbf{M}_c\|$ is less than 1, even though the target is close to the rough surface (distance = 0.25λ), and decreases when the distance increases. Comparing the three curves in each figure shows that with the decreasing of radius R of the cylinder, the norm lessens, as the coupling induction between the target and the rough surface reduces. Comparing the corresponding curves for each R (3λ , 6λ , 9λ) in two figures reveals that with the increasing of length L of the rough surface, the norm also becomes less, which is because for a fixed size of the cylinder target, when the size of the rough surface increases, the relative proportion of the target-surface coupling scattering component in the total scattering reduces. Hence, it can be concluded that the norm is mainly influenced by the target-surface coupling scattering. For defining the distance below which the method cannot be used (i.e., $\|\mathbf{M}_c\| > 1$), some other numerical results are also calculated by us and eventually, found that the lower limit value of the vertical distance between the target and rough surface should be around the value $\delta + \Delta x_s$ (i.e., $0.1\lambda + 0.1\lambda = 0.2\lambda$, Δx_s is the sampling step ($\approx 0.1\lambda$, i.e., $\approx 25\lambda/256$ or $100\lambda/1024$)).

Figure 4 shows the comparison of EPIL + FBM and MOM for BSC of the composite sense versus the scattering angle. The incident frequency f is 3 GHz, i.e., the wavelength λ is 0.1 m. The incident angle is 20° . The radius of the cylinder is $R = 8\lambda$. The depth of the cylinder is $D = 16\lambda$. The height rms δ of the rough surface is 0.1λ . The correlation length l of the rough surface is 1.0λ . The length L of the rough soil surface is 100λ . The moisture content m_v of the soil is 0.15. The volumetric sand content s_v is 51.5%. The volumetric

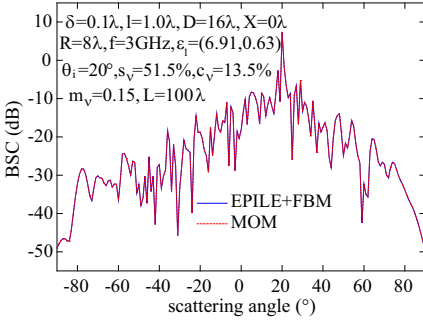


Figure 4. The BSC under $L = 100\lambda$.

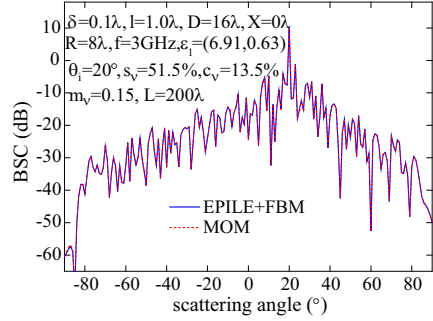


Figure 5. The BSC under $L = 200\lambda$.

clay content c_v is 13.5%. The temperature is 20°C. The permittivity calculated is $\varepsilon_1 = (6.91, 0.63)$ [30]. The number of samples for the cylinder target is 100, for the rough surface is 1024. One Monte-Carlo surface realization is averaged. In the EPILE, the number of iterations is 2. In the FBM, the number of iterations is 6. The RRE is 1.36733×10^{-6} , the CT by the EPILE + FBM is about 37 seconds (s), by the MOM (CGM) is 1 minute (min) 12 s. The curves match with each other. It can be considered that the ordered EPILE + FBM is basically exact and timesaving, compared with the MOM. Fig. 5 is the case that the length of the soil surface increases to 200λ and that the number of samples for it increases to 2048, while other parameters are fixed. The EPILE (2) + FBM (6) scheme is also applied. The CT by EPILE + FBM is 1 min 55 s, by MOM is 5 min 14 s, the RRE is 1.45174×10^{-5} . Comparing Fig. 5 with Fig. 4 indicates that the bigger the rough soil surface size is, the more evident the advantage of EPILE + FBM in computational time is, while the results are still basically exact.

We have also calculated the 2, 3 order EPILE combined with 2, 3, 4, 5, 6 order FBM. RRE and computational time (CT) are listed in Table 1. Comparison of the data in row suggests that for a given EPILE order, the RRE decreases as the FBM order increases and that the FBM increases one order, the CT increases 2 ~ 3 seconds. Comparing the data in column shows, for a given FBM order, the RRE decreases slightly as the EPILE order increases, and the EPILE increases one order, the CT increases 2 ~ 3 seconds. Comparing the data in column also demonstrates that for the same FBM order, the EPILE increases one order, the RRE is almost unchanged, hence, the RRE is mainly determined by the FBM order. The CT of EPILE (2) + FBM (3) almost equals that of the EPILE (3) + FBM (2).

Table 1. The comparison of different order EPILE combined with different order FBM in RRE and CT for one rough soil surface realization.

EPILE + FBM	(2) + (2)	(2) + (3)	(2) + (4)
RRE	<u>5.9040528</u>	<u>5.9546601</u>	<u>6.6093658</u>
	<u>66348593</u> $\times 10^{-3}$	<u>04794631</u> $\times 10^{-5}$	<u>54741271</u> $\times 10^{-6}$
CT	≈ 28 s	≈ 30 s	≈ 32 s
EPILE + FBM	(2) + (5)	(2) + (6)	(3) + (2)
RRE	<u>2.0294796</u>	<u>1.3673339</u>	<u>5.9040528</u>
	<u>50058633</u> $\times 10^{-6}$	<u>90203251</u> $\times 10^{-6}$	<u>66348482</u> $\times 10^{-3}$
CT	≈ 35 s	≈ 37 s	≈ 30 s
EPILE + FBM	(3) + (3)	(3) + (4)	
RRE	<u>5.9546601</u>	<u>6.6093658</u>	
	<u>04794571</u> $\times 10^{-5}$	<u>54741194</u> $\times 10^{-6}$	
CT	≈ 33 s	≈ 35 s	
EPILE + FBM	(3) + (5)	(3) + (6)	
RRE	<u>2.0294796</u>	<u>1.3673339</u>	
	<u>50058589</u> $\times 10^{-6}$	<u>90203244</u> $\times 10^{-6}$	
CT	≈ 38 s	≈ 41 s	

According to Table 1, it can also be found that the second order EPILE combined with sixth order FBM scheme (EPILE (2) + FBM (6)) is of reasonable accuracy and computational efficiency, hence, subsequently, the influence of parameters- R , D , δ , l , θ_i , m_ν , and X on the BSC using the EPILE (2) + FBM (6) will be investigated in turn and corresponding conclusions will be obtained.

Figure 6 exhibits the BSC versus the scattering angle for a cylinder target located below the exponential spectrum rough soil surface with different cylinder target radius using the EPILE + FBM. $N_t = 100$, $N_r = 1024$, $s_\nu = 51.5\%$ and $c_\nu = 13.5\%$. These and other parameters are also shown in the figure. The temperature is 20°C . 50 Monte-Carlo surface realizations are averaged. It is shown that with the increasing of the radius of the cylinder, the specular coherent scattering changes slightly, while the incoherent scattering at non-specular region

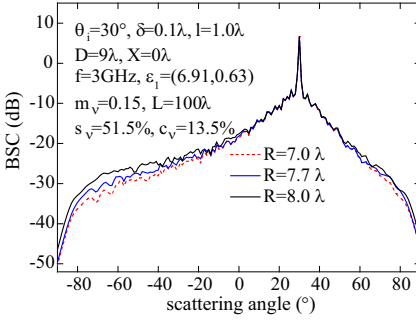


Figure 6. The BSC under different R .

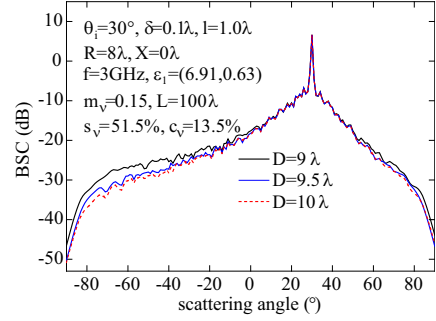


Figure 7. The BSC under different D .

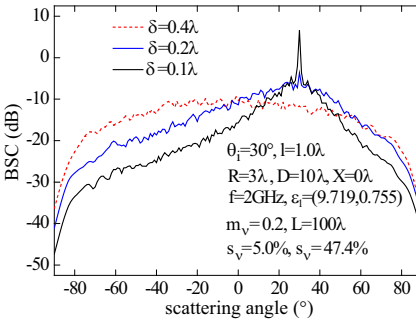


Figure 8. The BSC under different δ .

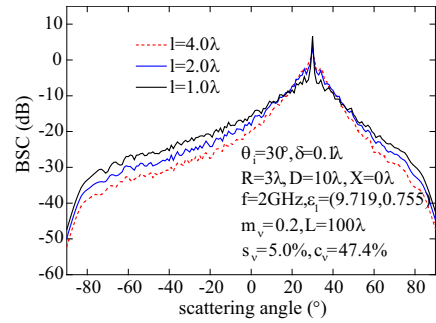


Figure 9. The BSC under different l .

increases evidently, especially at the backward scattering direction, as the coupling scattering between the target and the rough surface increases simultaneously. The dependency of the BSC on the depth D of the cylinder is depicted in Fig. 7. $N_t = 100$ and $N_r = 1024$. The temperature is 20°C . Other parameters are listed graphically. 50 Monte-Carlo surface realizations are counted. It can be found that with the increasing of depth of cylinder, the specular coherent scattering changes slightly, while the incoherent scattering at non-specular region decreases evidently, especially at the backward direction, owing to the decreasing coupling scattering between the target and rough soil surface.

In Fig. 8, using the EPILÉ + FBM, the influence of rms height δ of soil surface on BSC of the composite model is investigated. $N_t = 100$, $N_r = 1024$, $s_v = 5.0\%$ and $c_v = 47.4\%$. The temperature is 20°C . Parameters are also listed in figure (50 surface realizations). Obviously, with the increasing of rms height δ , the specular coherent

scattering decreases, while the incoherent scattering at non-specular direction increases evidently, especially at the backward direction, as the bigger the rms height is, the soil surface is rougher, hence, the coupling scattering between the target and the rough surface are more. Fig. 9 gives the dependence of correlation length l on the BSC using EPILE + FBM for 50 surface realizations. $N_t = 100$, $N_r = 1024$, $s_\nu = 5.0\%$ and $c_\nu = 47.4\%$. The temperature is 20°C . Evidently, with the increasing of the correlation length, the specular coherent scattering decreases, but the specular peak becomes wider, the incoherent scattering at non-specular direction decreases, as the bigger the rms height is, the smoother the soil surface is, hence, the less the coupling scattering between the target and rough surface is.

To further explore the important scattering characteristics of the composite model, in Fig. 10, using the EPILE + FBM, the BSC of averaging 50 soil surfaces is examined for different incident angles 30° , 45° , 60° , respectively. $N_t = 100$, $N_r = 1024$, $s_\nu = 5.0\%$ and $c_\nu = 47.4\%$. The temperature is 20°C . It can be observed that with the increasing of the incident angle, the specular coherent scattering decreases, while the width of the specular peak becomes wider. With the changing of the soil moisture m_ν , the BSC by the EPILE + FBM for 50 soil surfaces is investigated in Fig. 11. $N_t = 100$, $N_r = 1024$, $s_\nu = 17.2\%$ and $c_\nu = 19.0\%$. The temperature is 20°C . With the increasing of soil moisture content, the real part of the permittivity increases, and visually, the specular coherent scattering increases, the incoherent scattering at non-specular region also changes evidently. The dependency of the BSC (50 surface realizations) on horizontal distance X is also shown in Fig. 12. $N_t = 100$, $N_r = 1024$, $s_\nu = 17.2\%$ and $c_\nu = 19.0\%$. The temperature is 20° . It is indicated that with the increasing X , the scattering curve decreases at non-specular region,

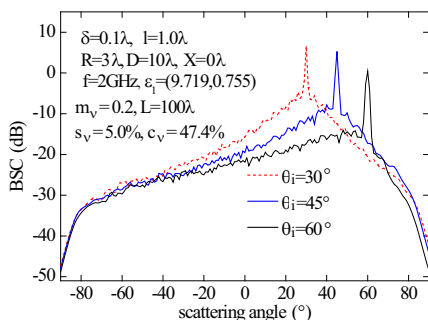


Figure 10. The BSC under different θ_i .

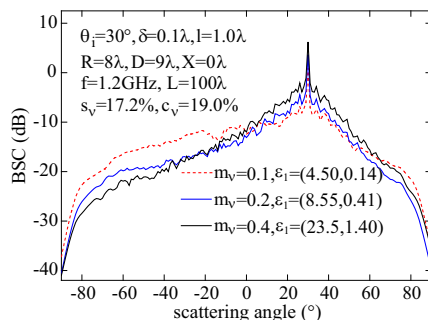


Figure 11. The BSC under different m_ν .

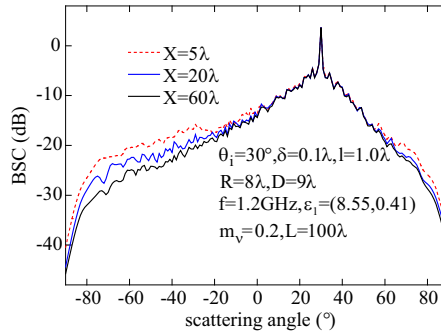


Figure 12. The BSC under different X .

especially at backward region, because the intensity of the Thorsos' tapered wave decreases gradually from the center to the edge of the soil surface (as shown in Fig. 1), hence, the coupling scattering from the cylinder and the rough soil surface is the strongest when the X adjoins the center of the rough soil surface, and decreases gradually when horizontal distance X close to its extremities.

7. CONCLUSIONS

In this paper, the numerical scheme EPILÉ + FBM is applied to study the composite scattering from target below the dielectric rough soil surface. This method is based on the rigorous PILE and the Forward-Backward method. Using this scheme, the scattering from the cylinder target below the exponential spectrum rough soil surface is investigated. With the increasing size of soil surface, the EPILÉ + FBM can reduce the complexity. Generally speaking, within the iteration order ≤ 5 , the minimum RRE for the EPILÉ + FBM is about 10^{-6} quantity level, i.e., the basically exact results can be obtained by this method only through a few iterations, while the computing efficiency is improved (more evident when surface size increases), compared with MOM (CGM). If iteration order increases, the RRE will decrease further. When the EPILÉ order is fixed, the RRE decreases with the increasing of FBM order. When the EPILÉ order is fixed, if the FBM increases one order, the CT increases 2 ~ 3 seconds. When the FBM order is fixed, if the EPILÉ increases one order, the CT increases 2 ~ 3 seconds. With the increasing of radius of cylinder, the BSC increases at large scattering angle. With the increasing of depth of cylinder, the BSC decreases at large scattering angle. With the increasing of rms height, the BSC decreases at specular direction and increases at large scattering angle. With the increasing

of correlation length, the BSC decreases both at specular and non-specular direction, while the specular peak becomes wider. With the increasing of incident angle, the BSC decreases at specular direction, while the width of specular peak becomes wider. With the increasing of soil moisture content, the real part of permittivity increases and the BSC increases at specular direction. With the increasing horizontal distance of target, the incoherent scattering decreases gradually. The presented scheme is meaningful for the topics related with the composite scattering characteristics extraction, passive remote sensing and electromagnetic inverse scattering problem, most of which are carried out based on the acquisition of plenty of calculated data under multi-parameters in a more efficient extent. Based on this scheme, our future work will focus on the further investigation of the buried object detection [35] and passive remote sensing [36], owing to their potential application in ground-penetrating radar, military, landmine detection, and environment remote sensing etc.

ACKNOWLEDGMENT

This work was supported by the Science Foundation of Yangzhou University (Grant No. 2012CXJ009), the National Natural Science Foundation for Distinguished Young Scholars of China (Grant No. 61225002), the Specialized Research Fund for the Doctoral Program of Higher Education (Grant No. 20100203110016). The authors would like to thank the reviewers for their constructive suggestions.

REFERENCES

1. Rice, S. O., *Reflection of Electromagnetic Waves from Slightly Rough Surfaces, in Theory of Electromagnetic Waves*, M. Kline, Ed., 351–378, Wiley, New York, 1951.
2. Holliday, D., “Resolution of a controversy surrounding the Kirchhoff approach and the small perturbation method in rough surface scattering theory,” *IEEE Trans. on Antennas and Propag.*, Vol. 35, No. 1, 120–122, Jan. 1987.
3. Wu, Z. S., J. P. Zhang, L. X. Guo, and P. Zhou, “An improved two-scale model with volume scattering for the dynamic ocean surface,” *Progress In Electromagnetics Research*, Vol. 89, 39–56, 2009.
4. Winebrenner, D. and A. Ishimaru, “Investigation of a surface field

- phase perturbation technique for scattering from rough surfaces,” *Radio Sci.*, Vol. 20, No. 2, 161–170, 1985.
5. Luo, G. and M. Zhang, “Investigation on the scattering from one-dimensional nonlinear fractal sea surface by second-order small-slope approximation,” *Progress In Electromagnetics Research*, Vol. 133, 425–441, 2013.
 6. Lentz, R. R., “A numerical study of electromagnetic scattering from ocean-like surfaces,” *Radio Sci.*, Vol. 9, 1139–1146, 1974.
 7. Chan, C. H., S. H. Lou, L. Tsang, and J. A. Kong, “Electromagnetic scattering of waves by random rough surface: A finite-difference time-domain approach,” *Micro. Opt. Tech. Lett.*, Vol. 4, No. 9, 355–359, 1991.
 8. Lou, S. H., L. Tsang, and C. H. Chan, “Application of finite element method to Monte Carlo simulations of scattering of waves by random rough surfaces: Penetrable case,” *Waves in Random Media*, Vol. 1, No. 4, 287–307, 1991.
 9. Tsang, L., C. H. Chang, H. Sangani, A. Ishimaru, and P. Phu, “A banded matrix iterative approach to monte carlo simulations of large scale random rough surface scattering: TE case,” *Journal of Electromagnetic Waves and Applications*, Vol. 7, No. 9, 1185–1200, 1993.
 10. Iodice, A., “Forward-backward method for scattering from dielectric rough surfaces,” *IEEE Trans. on Antennas and Propag.*, Vol. 50, No. 7, 901–911, 2002.
 11. Jandhyala, V., E. Michielssen, S. Balasubramaniam, and W. C. Chew, “A combined steepest descent-fast multipole algorithm for the fast analysis of three-dimensional scattering by rough surfaces,” *IEEE Trans. on Geosci. Remote Sens.*, Vol. 36, No. 3, 738–748, 1998.
 12. Qi, C., Z. Zhao, W. Yang, Z. P. Nie, and G. Chen, “Electromagnetic scattering and doppler analysis of three-dimensional breaking wave crests at low-grazing angle,” *Progress In Electromagnetics Research*, Vol. 119, 239–252, 2011.
 13. Dusséaux, R., E. Vannier, O. Taconet, and G. Granet, “Study of backscatter signature for seedbed surface evolution under rainfall-influence of radar precision,” *Progress In Electromagnetics Research*, Vol. 125, 415–437, 2012.
 14. Wang, X., C. F. Wang, and Y. B. Gan, “Electromagnetic scattering from a circular target above or below rough surface,” *Progress In Electromagnetics Research*, Vol. 40, 207–227, 2003.
 15. Wang, X. and L. -W. Li, “Numerical characterization of bistatic

- scattering from PEC cylinder partially embedded in a dielectric rough surface interface: Horizontal polarization,” *Progress In Electromagnetics Research*, Vol. 91, 35–51, 2009.
16. Guo, L. X., A. Q. Wang, and J. Ma, “Study on EM wave scattering from 2-D target above 1-D large scale rough surface with low grazing incidence by parallel MOM based on PC clusters,” *Progress In Electromagnetics Research*, Vol. 89, 149–166, 2009.
 17. Jin, Y. Q. and G. Li, “Detection of a scatter target over a randomly rough surface by using the angular correlation function in a finite-element approach,” *Waves in Random Media*, Vol. 10, No. 4, 273–280, 2000.
 18. Chan, C. H., S. H. Lou, L. Tsang, and J. A. Kong, “Electromagnetic scattering of waves by random rough surface: A finite-difference time-domain approach,” *Micro. Opt. Tech. Lett.*, Vol. 4, No. 9, 355–359, 1991.
 19. Zhang, Y., Y. E. Yang, H. Braunisch, and J. A. Kong, “Electromagnetic wave interaction of conducting object with rough surface by hybrid SPM/MOM technique,” *Progress In Electromagnetics Research*, Vol. 22, 315–335, 1999.
 20. Ye, H. and Y. Q. Jin, “A hybrid KA-MoM algorithm for computation of scattering from a 3-D PEC target above a dielectric rough surface,” *Radio Sci.*, Vol. 43, No. 3, 56–70, 2008.
 21. He, S. Y. and G. Q. Zhu, “A hybrid MM-PO method combining UV technique for scattering from two-dimensional target above a rough surface,” *Micro. Opt. Tech. Lett.*, Vol. 49, No. 12, 2957–2960, 2007.
 22. Chiu, T. and K. Sarabandi, “Electromagnetic scattering interaction between a dielectric cylinder and a slightly rough surface,” *IEEE Trans. on Antennas and Propag.*, Vol. 47, No. 10, 902–913, 1999.
 23. Pino, M. R., L. Landesa, J. L. Rodriguez, F. Obelleiro, and R. J. Burkholder, “The generalized forward-backward method for analyzing the scattering from targets on ocean-like rough surfaces,” *IEEE Trans. on Antennas and Propag.*, Vol. 47, No. 6, 961–968, 1999.
 24. Liang, Y., L. X. Guo, and Z. S. Wu, “The EPILC combined with the generalized-FBM for analyzing the scattering from targets above and on a rough surface,” *IEEE Antennas Wireless Propag. Lett.*, Vol. 9, No. 6, 809–813, 2010.
 25. Zhang, Y., J. Lu, J. Pacheco, Jr., C. D. Moss, C. O. Ao, T. M. Grzegorzcyk, and J. A. Kong, “Mode-expansion method for calculating electromagnetic wave scattered by object on rough

- ocean surface," *IEEE Trans. on Antennas and Propag.*, Vol. 53, No. 5, 1631–1639, 2005.
26. Ye, H. and Y. Q. Jin, "Fast iterative approach to difference scattering from the target above a rough surface," *IEEE Trans. on Geosci. Remote Sens.*, Vol. 41, No. 1, 108–115, 2006.
 27. Xu, F. and Y. Q. Jin, "Bidirectional analytic ray tracing for fast computation of composite scattering from electric-large target over a randomly rough surface," *IEEE Trans. on Antennas and Propag.*, Vol. 57, No. 5, 1495–1505, 2009.
 28. Déchamps, N., N. de Beaucoudrey, C. Bourlier, and S. Toutain, "Fast numerical method for electromagnetic scattering by rough layered interfaces: Propagation-inside-layer expansion method," *J. Opt. Soc. Amer. A*, Vol. 23, No. 2, 359–369, 2006.
 29. Kubické, G., C. Bourlier, and J. Saillard, "Scattering by an object above a randomly rough surface from a fast numerical method: Extended PILE method combined with FB-SA," *Waves in Random and Complex Media*, Vol. 18, No. 3, 495–519, 2008.
 30. Wang, J. R. and T. J. Schmugge, "An empirical model for the complex dielectric permittivity of soils as a function of water content," *IEEE Trans. on Geosci. Remote Sens.*, Vol. 18, No. 4, 288–295, 1980.
 31. Tsang, L. and J. A. Kong, *Scattering of Electromagnetic Waves-numerical Simulations*, 114–176, Wiley, New York, 2000.
 32. Thorsos, E. I., "The validity of the Kirchhoff approximation for rough surface scattering using a Gaussian roughness spectrum," *J. Acous. Soc. Am.*, Vol. 83, No. 1, 78–92, 1988.
 33. Hestenes, M. R. and E. Stiefel, "Method of conjugate gradients for solving linear systems," *J. Res. Natl. Bur. Stand.*, Vol. 49, No. 2, 409–436, 1952.
 34. Liang, Y., L. X. Guo, and Z. S. Wu, "The fast EPILE combined with FBM for electromagnetic scattering from dielectric targets above and below the dielectric rough surface," *IEEE Trans. on Geosci. Remote Sens.*, Vol. 49, No. 10, 3892–3905, 2011.
 35. Zhu, X., Z. Zhao, W. Yang, Y. Zang, Z. Nie, and Q. H. Liu, "Iterative time-reversal mirror method for imaging the buried object beneath rough ground surface," *Progress In Electromagnetics Research*, Vol. 117, 19–33, 2011.
 36. Xu, P., L. Tsang, and K. S. Chen, "Fourth stokes parameter in polarimetric passive remote sensing from two-layer rough surfaces," *Progress In Electromagnetics Research*, Vol. 129, 125–141, 2012.